Modeling the Relaxation Time of DNA Confined in a Nanochannel

Douglas R. Tree,[1] Yanwei Wang,[2, a)] and Kevin D. Dorfman[1, b)]

[1)] *Department of Chemical Engineering and Material Science, University of Minnesota – Twin Cities, 421 Washington Ave SE, Minneapolis, Minnesota 55455, USA*

[2)] *Department of Polymer Science and Engineering, College of Chemistry, Chemical Engineering and Materials Science, Soochow University, 199 Ren-ai Road, Suzhou 215123, People's Republic of China*

Using a mapping between a Rouse dumbbell model and fine-grained Monte Carlo simulations, we have computed the relaxation time of λ-DNA in a high ionic strength buffer confined in a nanochannel. The relaxation time thus obtained agrees quantitatively with experimental data (Reisner *et al.*, *Phys. Rev. Lett.* **2005**, *94*, 196101) using only a single $O(1)$ fitting parameter to account for the uncertainty in model parameters. In addition to validating our mapping, this agreement supports our previous estimates of the friction coefficient of DNA confined in a nanochannel (Tree *et al.*, *Phys. Rev. Lett.* **2012**, *108*, 228105), which have been difficult to validate due to the lack of direct experimental data. Furthermore, the model calculation shows that as the channel size passes below approximately 100 nm (or roughly the Kuhn length of DNA) there is a dramatic drop in the relaxation time. Inasmuch as the chain friction rises with decreasing channel size, the reduction in the relaxation time can be solely attributed to the sharp decline in the fluctuations of the chain extension. Practically, the low variance in the observed DNA extension in such small channels has important implications for genome mapping.

PACS numbers: 87.15.ak, 87.14.gk

[a)]Electronic mail: ywwang@suda.edu.cn

[b)]Electronic mail: dorfman@umn.edu

I. INTRODUCTION

The extension of a long DNA molecule confined in a nanochannel has attracted tremendous attention[1–4] in large part because it couples a fundamental polymer physics problem to an important application in genomics, namely DNA barcoding[5–9]. The theoretical basis for the equilibrium extension of DNA in a nanochannel has been addressed to varying degrees of accuracy by theory and simulation for strong[5,10–18], moderate[17,19–32] and relatively weak[33–36] confinement, leading to the reconciliation[26,30] between early experimental observations[37] and the predictions of the classic theories from Odijk[10] and de Gennes[33]. Due to both the paucity of dynamic data in strong confinement and the computational difficulty of simulating the dynamics of long chains, there is little work validating the computational predictions of confined DNA dynamics in nanochannels with hydrodynamic interactions[38]. We show here that the confined wormlike chain model used to model DNA extension can explain experimental results[37,39] for the relaxation time of a long DNA molecule in a nanochannel. Furthermore, our simulations highlight a previously overlooked strong reduction in the relaxation time as the channel size is reduced below the Kuhn length of the DNA, which has practical implications for the practice of DNA barcoding[7].

It is not trivial to compute the relaxation time of a long polymer in confinement. In addition to obvious challenges in computing the hydrodynamics of confined polymers[40], one of the major challenges in modeling DNA in a nanochannel is selecting a model that can accommodate the large separation of length and time scales. Explicitly, the effective width of the polymer backbone, w, is small compared to the persistence length, l_p, which itself is small compared to the contour length, L, of the chain. The nanochannel width introduces a fourth length scale, D, with the ratio D/l_p determining the strength of the confinement. In very weak confinement ($D \gg l_p$) it is possible to use a coarse-grained, bead-spring model[34] parameterized to match experimental data[41,42]. However, this model cannot resolve DNA deformation when the confinement length scale approaches the undeformed size of one (Gaussian) "spring" of DNA. A natural solution to the resolution problem is to use a fine-scale model, such as the wormlike osculating-sphere model (WOSM)[30,38,43,44], where the DNA is modeled by a string of beads of size w interacting via a discrete wormlike chain bending potential[11] and hard core excluded volume. This model can easily capture confinement down to the strong confinement regime ($D \ll l_p$), provided that we simultaneously ensure that the

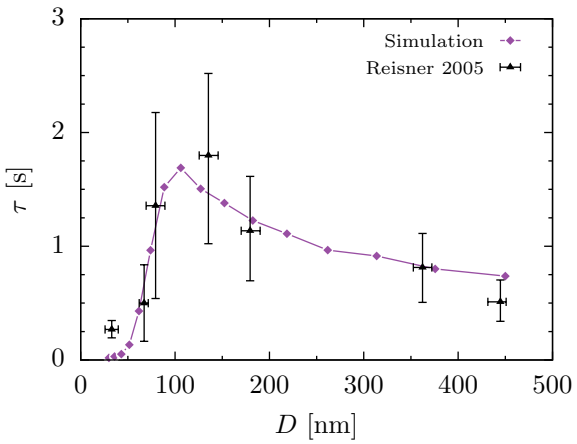

FIG. 1. Relaxation time (purple diamonds) obtained from Eq. 5 with $c = 1.2$ and the WOSM compared to the experimental data of Reisner *et al.*[37] (black triangles).

bond length, which is the bead size w for the WOSM, is small compared to the channel size to avoid discretization artifacts[30]. These are not the only two model options; for example, the discrete stretchable, shearable wormlike chain model[45] represents an attractive choice, but the dynamical implementation of this model for complicated problems remains a work in progress. There are other options for simulating confined polymers that are well suited to examining scaling laws, such as the bond fluctuation method[46], but these models are challenging to connect quantitatively to the experimental parameters.

For double-stranded DNA in nanochannels in a high ionic strength buffer, it is now accepted that most experiments are carried out in the crossover regime between the classical de Gennes regime[33] (suitable for $l_p^2/w < D < R_g$[21,26], where R_g is polymer's radius of gyration in free solution) and Odijk regime[10] (suitable for $D \ll l_p$). These circumstances necessitate a fine-scale representation such as the WOSM. However, a typical molecule such as λ-DNA (48,500 base pairs) requires simulation of several thousand beads and the longer molecules used for genomic mapping[7] require tens of thousands of beads. Dynamic simulations become extremely expensive with high spatial discretization and large molecular weights, even with fast implicit solvent methods for the hydrodynamic interactions in confinement[40].

Fortunately, it is possible to arrive at a reasonable estimate for the polymer relaxation time, τ, by mapping the chain dynamics to a one-dimensional, overdamped, Rouse dumbbell model with a finite but non-zero equilibrium extension[47,48]. In the present contribution, we show how the Monte Carlo methods used in our previous work to compute the extension[26,30]

and the hydrodynamic mobility[38] can be used to parameterize such a dumbbell model. The ultimate result of our analysis is seen in Fig. 1, which compares our computational predictions to the seminal experiments of Reisner *et al.*[37]. The agreement between our approach and the experimental results shown in Fig. 1 lend confidence to our use of the WOSM, the Kirkwood approximation employed to obtain the friction, and the assumptions made in mapping the model to an overdamped, Rouse dumbbell. Furthermore, this agreement provides a basis for considering the WOSM model in the engineering of nanochannel devices for genomic mapping. However, there are certainly limitations to the computational model and gaps in our understanding of the underlying physics, which are discussed in conjunction with our modeling results.

II. METHODS

A. Dumbbell Model and Mapping

We begin by recalling the physics required to map the chain dynamics to a one-dimensional, overdamped, Rouse dumbbell model with a finite equilibrium extension[47,48]. In this model, the autocorrelation function $C(t)$ of the fluctuation about the mean extension $\langle X \rangle$ is given by[49]

$$C(t) = \langle \delta_X(0)\delta_X(t) \rangle = \langle \delta_X^2 \rangle \exp(-t/\tau) \tag{1}$$

where

$$\delta_X(t) \equiv X(t) - \langle X \rangle \tag{2}$$

is the deviation from the mean extension and

$$\tau = \frac{\zeta}{2k_{\text{eff}}} \tag{3}$$

is the relaxation time. Two important terms appear in Eq. 3: ζ, the friction coefficient of each of the two beads comprising the dumbbell and k_{eff}, the spring constant of the Hookean spring between them[47,48].

To map between the two models, both the friction coefficient, ζ, and the effective spring constant, k_{eff}, of the dumbbell model must be defined in terms of the wormlike chain model. Since the dumbbell model has no hydrodynamic interactions, the friction of the center-of-mass of the dumbbell is simply equal to 2ζ. Equating the center-of-mass friction of the

WOSM to that of the dumbbell defines ζ and provides the first part of the map. Per this definition, the dumbbell friction is independent of conformation fluctuations. This is appropriate, since the friction coefficient obtained from the WOSM employs a rigid-body approximation[50,51] similar to the mean field pre-averaging approximation used in the Zimm model[47]. Accordingly, we focus on the case when the conformation is unperturbed by external forces (other than confinement). This means the relaxation time obtained by this method is only valid for the fluctuations of the polymer about its equilibrium conformation. We thus do not consider the possibility of a second relaxation time related to non-equilibrium stretching[52].

The spring constant of the Rouse dumbbell is obtained from the equipartition theorem, which gives

$$k_{\text{eff}} = \frac{k_B T}{\langle \delta_X^2 \rangle} \tag{4}$$

where k_B is Boltzmann's constant, T is the absolute temperature and $\langle \delta_X^2 \rangle$ is the variance in the extension of the spring. Since the spring is harmonic, the probability density function of the extension in the dumbbell model is Gaussian[47], and is therefore completely described by the mean span, $\langle X \rangle$, and variance $\langle \delta_X^2 \rangle$. Subsequently, the first two moments of the extension distribution function in the WOSM are used to define the dumbbell harmonic spring and are thus sufficient to define the effective spring constant. This implies that the spring constant mapping is only valid insofar as the extension distribution function is well described by its first two moments. This certainly breaks down for extensions near the maximum contour length and cases where the extension distribution is complicated or multi-modal as might exist in the presence of backfolded states in tight confinement[17,20,29]. Note that for the chain extension we chose to work in terms of the span, X[53], rather than the end-to-end distance, since the former is the experimentally relevant metric.

In the light of this mapping, it proves convenient to recast Eq. 3 in terms of the quantities obtainable from the simulation of the WOSM. With this change of variables, the relaxation time becomes

$$\frac{\tau}{\tau_{\text{R}}} = \frac{c}{4} \frac{\langle \delta_X^2 \rangle}{L l_p} \frac{2\zeta}{\eta L} \tag{5}$$

where

$$\tau_{\text{R}} \equiv \frac{\eta L^2 l_p}{k_B T} \tag{6}$$

is the Rouse relaxation time for an ideal chain without the prefactor[54,55]. In Eq. 5, we

included a prefactor c as an $O(1)$ fitting parameter that we will use in the subsequent analysis. Note that $c = 4/\pi^2$ would be an appropriate choice resulting from matching the center of mass diffusivity of a Rouse chain to a dumbbell model[49].

While a simple dumbbell model may seem like a very crude approximation, a single exponential decay of $C(t)$ is consistent with experimental findings[3,37]. Furthermore, we do not construct the dumbbell arbitrarily; instead, it is parameterized to match equilibrium properties determined from Monte Carlo sampling of the fine-scale WOSM. This strategy gives nearly quantitative agreement between the simulation results and experimental data for the relaxation time with a single $O(1)$ fitting parameter to account for the uncertainty in the various physical parameters appearing in the detailed model.

B. Monte Carlo Simulations

To parameterize the dumbbell model, we employ the aforementioned WOSM in a square nanochannel of size D as described in our previous publications[30,38,56]. To compute equilibrium chain properties, we used a standard Metropolis algorithm with reptation and crankshaft moves[26]. To calculate the values of ζ and $\langle \delta_X^2 \rangle$ which we desire, we require a fully parameterized WOSM, which includes an effective width, w, a persistence length, l_p, a contour length, L, and a hydrodynamic radius, a[56]. As the aim of our simulations is ultimately a comparison with the experimental relaxation time data from Reisner *et al.*[37], we examine λ-DNA in channel sizes between 30 nm and 450 nm. We approximate the dyed contour length of λ-DNA as $L = 18.63$ μm, as suggested by these authors[37], which is within the sizes we can compute using the standard Metropolis algorithm[30,38].

In addition to the channel size and contour length, the model requires specifying the persistence length, which parameterizes the bending energy, and an effective width of the DNA, which parameterizes both the hard core, intrachain excluded volume interactions and the hardcore interactions with the channel walls. Note that in the WOSM the discretization length equals the effective width making the total contour length equal to the number of beads times the effective width. While there is widespread agreement that the persistence length of double-stranded DNA in a high ionic strength buffer is approximately 50 nm[57], there is less consensus surrounding the effective width.

In our previous work[26], we suggested treating the effective width as a free parameter to fit

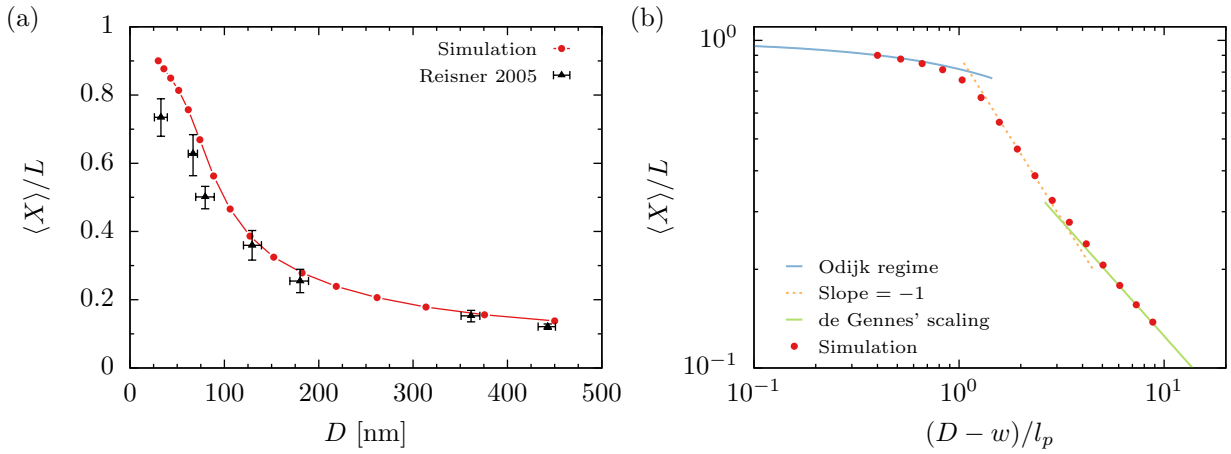

FIG. 2. (a) Fractional extension of DNA in a square nanochannel of size D from Monte Carlo simulations (red circles) and from Reisner *et al.*[37] (black triangles). Error bars for the simulation data are the standard error, and when not explicitly shown, the error is of order of the symbol size. Simulation parameters: $l_p = 50$ nm, $w = 10$ nm, $L = 18.63$ μm (i.e. 1863 spheres). The same set of parameters is used throughout this work. (b) Same data plotted in dimensionless log-log form. The solid blue line is the prediction for the Odijk regime[10] with no free parameters[14]. The dashed line is the predicted slope for the proposed Gauss-de Gennes regime[30], and the solid green line is the scaling $D^{1-1/\nu}$ with $\nu = 0.5876$.

the simulation data for $\langle X\rangle$ to experimental data, provided that the end result is reasonably close to the prediction from Stigter's theory for short, rod-like DNA[58]. (For high ionic strengths, Stigter's theory[58] predicts $w \approx 5$ nm.) In our initial foray into this problem,[26] we concluded that an effective width between 4.6 nm and 12 nm seemed reasonable, with $w = 7$ nm being the best fit for the experimental extension data[37] after trying to collapse it with de Gennes scaling. Given the uncertainty in the exact value of the effective width, especially the difference between DNA-DNA interactions and DNA-wall interactions, we decided to take a simple, approximate approach in our work here. We set the effective width to be $w = 10$ nm and combine this with an estimate of the persistence length with a single significant digit as well, $l_p = 50$ nm. These are reasonable order-of-magnitude estimates for both parameters, and we conjecture that the adjustable parameter c in Eq. 5 will ultimately allow us to correct for the uncertainty.

Figure 2(a) shows the WOSM mean span versus channel size compared to the exper-

imental data of Reisner *et al.*[37], which justifies our supposition regarding the parameter estimates. There is very good agreement between the model predictions and the experimental data for large channel sizes, where we observe de Gennes scaling and expect excluded volume to play a significant role[30]. However, for small channels, the WOSM values deviate significantly from the experimental data, suggesting that as the channel size approaches the effective width, hardcore interactions between the polymer and channel become increasingly inadequate to describe the real system. We should also point out that the experimental data were obtained in rectangular channels[37], and there is a small correction for the channel aspect ratio[26] that is not incorporated into our analysis.

Figure 2(b) shows that the extension results are also consistent with the scaling produced by prior simulation work. In the region $D/l_p \sim 1$, we observe a slope D^{-1} that is consistent with extant simulation data by multiple groups[23,24,26,30] and the existence of a Gauss-de Gennes regime[30]. For the larger channel sizes, the scaling for the extension switches to $D^{1-1/\nu}$ with $\nu = 0.5877$. The latter result is consistent with either a de Gennes regime[33] or an extended de Gennes regime[19,26].

In addition to equilibrium values, we are interested in the chain friction, ζ, which is determined by a rigid-body approximation to the diffusivity[43,59]. Specifically, similar to our previous work[38], the chain conformations used to obtain Fig. 2 are combined with a numerically determined confined hydrodynamics tensor[34]. The confined hydrodynamic tensor leaves a degree of freedom for the bead hydrodynamic radius, a. Our recent analysis of the free solution diffusivity of DNA[56] indicates that for a touching *hydrodynamic* bead model, a value of $a = 3$ nm gives a good approximation of the diffusivity. We use this value, noting that the WOSM model does not have touching hydrodynamic beads, which introduces some error. Doing so, we again anticipate that the value of c in Eq. 5 will compensate for the error introduced here.

Before proceeding, we should also justify the need for the new Monte Carlo simulations presented here in the light of our previous work. In principle, we could use our existing simulation data for short chains[26,30,38] and then extrapolate to λ-DNA using scaling laws. However, since these scaling laws are implicitly one of the things we are trying to evaluate, such an approach seems questionable. The new calculations we used here are intended to provide data at the molecular weight of λ-DNA and cover the full range of channel sizes used in experiments[37]. We thus expect the trends in the mean span[26,30] and hydrodynamic

mobility[30] as a function of confinement to be identical to our prior results, even if the quantitative values may differ slightly. For instance, the parameters used in Fig. 2 correspond to a monomer anisotropy $\epsilon \equiv w/l_p = 0.2$. In our recent work on the Gauss-de Gennes regime[30], we pointed out that the Gauss-de Gennes scaling $\langle X \rangle \sim D^{-1}$ results from the stiffness of the chain, much in the way that the range of molecular weights that exhibit ideal chain scaling for the free solution radius of gyration increases with monomer anisotropy. Using scaling arguments, we showed that the range of channel sizes in the Gauss-de Gennes regime increases with increasing monomer anisotropy, and that this regime should disappear entirely in the limit of a freely jointed chain. The relatively flexible chain model used here suppresses the extent of the Gauss-de Gennes scaling $\langle X \rangle \sim D^{-1}$, which is reflected in the data in Fig. 2.

Additionally, we have also computed new results for the variance in the extension (span) of the chain, a parameter appearing in the dumbbell model, and (in Section III B) we confirm that the span distributions are reasonably Gaussian, which is an assumption in the dumbbell model. The variance of the span has yet to be systematically studied as a function of confinement and monomer anisotropy, although there are some intriguing new results supporting the existence of an extended de Gennes regime[32]. In fact, all of the physical quantities required to arrive at the relaxation time (average extension, variance in the extension, and the hydrodynamic mobility) depend on the extent of confinement and the physical properties of DNA, and a complete understanding of these relationships has yet to be achieved[3]. Thus, while there are deep scientific insights to be mined by exploring these dependencies in detail, for this work we keep our focus very practical — we simply want to show that models and methodologies now exist to determine the relaxation time of channel-confined DNA, and carefully assess the limitations of this approach.

III. RESULTS AND DISCUSSION

A. Computing the relaxation time

Figure 3 shows Metropolis Monte Carlo results for the variance in the extension, $\langle \delta_X^2 \rangle$, and the chain friction, ζ, as a function of channel size for λ-DNA. The friction and mean span fluctuations in Fig. 3 along with the parameters necessary to define τ_R provide the

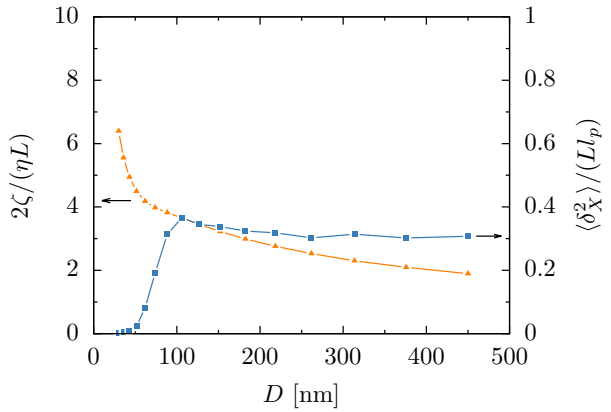

FIG. 3. Normalized chain friction (left panel, orange triangles) and normalized fluctuations in the mean span (right panel, blue squares) of the WOSM as a function of channel size.

necessary data to compute the relaxation time via Eq. 5. Using the aforementioned contour and persistence lengths and assuming a viscosity of 1 cP and a temperature of 298 K gives $\tau_R \approx 4.2$ s. Combining these results with the choice $c = 1.2$ gives the relaxation times shown in Fig. 1, which are compared to the experimental data reported by Reisner *et al.*[37].

The friction coefficient appearing in Fig. 3 behaves as expected, given previous computational results for the mobility of semiflexible chains in confinement[38]. In weak confinement, the friction slowly increases as the channel size decreases, consistent with a blob theory. In strong confinement, the friction diverges logarithmically, consistent with a lubrication model for the relative motion of concentric cylinders. From this we conclude that these previously observed[38] trends are robust to the molecular weight, persistence length and effective width used here.

The variance, on the other hand, shows more interesting behavior. The data show a small, gradual increase in the variance as the channel size decreases until the channel size is around the Kuhn length of DNA (100 nm). Although we are focusing primarily on the approach required to produce Fig. 1, it is worthwhile to make a brief diversion here to discuss the relatively flat response of the channel fluctuations for $D > 100$ nm. In a recent publication, Dai and Doyle[32] proposed that the fluctuations in the chain extension are given by

$$\langle \delta X^2 \rangle \cong N_{\text{blob}} R_{\text{blob}}^2 \tag{7}$$

where N_{blob} is the number of blobs and R_{blob} is the size of the blob. The ideas behind this equation are that (i) the fluctuation of each blob is independent of the other blobs and (ii)

the influence of confinement inside a blob is negligible. Their analysis then suggests that the fluctuations in the extended de Gennes regime[19] should have the scaling[32]

$$\langle \delta X^2 \rangle \cong L l_p \tag{8}$$

which agrees with the result obtained from Flory theory[26] for the extended de Gennes regime. Interestingly, this logic also leads to the same scaling for the Gauss-de Gennes regime[30] if blob theory is indeed valid there. In the latter regime, the blob size is the channel size,

$$R_{\text{blob}} \cong D \tag{9}$$

The blobs are assumed to exhibit ideal chain statistics[22,30,33,60]

$$L_{\text{sub}} l_p \cong D^2 \tag{10}$$

where L_{sub} is the contour length of the subchain inside a blob. The total number of blobs is then

$$N_{\text{blob}} = \frac{L}{L_{\text{sub}}} \cong \frac{L l_p}{D^2} \tag{11}$$

Using Eq. 9 and Eq. 11 in Eq. 7 yields the same scaling for the extension fluctuations in the extended de Gennes regime (Eq. 8) and the Gauss-de Gennes regime.

Regardless of the specifics of the regime, the lack of dependence of the variance on the relaxation time means that, in moderate confinement, the relaxation time is especially sensitive to the friction coefficient. As a result, the qualitative agreement between the calculated and experimental relaxation times appearing in Fig. 1 provides evidence that, in moderate confinement, the rigid-body assumptions used to obtain the friction coefficient are adequate. While this evidence is not as strong as a direct experimental measurement of the chain friction coefficient, it is still a significant result given the difficulty in obtaining both experimental and computational data for the dynamics of moderately confined semiflexible chains.

As the channel size is decreased further and falls below the Kuhn length, the variance quickly drops, presumably due to the loss of the degrees of freedom associated with short length-scale backfolds along the chain contour[10,13,14,17,29]. As stated above, unlike the variance in the extension, the friction diverges as the channel size decreases. Thus for strong confinement, the variance in the mean span dominates the relaxation time.

Since the two curves present in Fig. 3 are directly combined to give the relaxation time in Fig. 1, we can assess the effect of both the friction and the variance in the extension on the relaxation time. We turn our attention back to Fig. 1 to do so. Note that the overall shape of the calculated and experimental relaxation time curves in Fig. 1 are similar, including the presence of a maximum in the relaxation time near the Kuhn length. Given our assessment of Fig. 3, we postulate that this maximum results from a tradeoff of increasing friction and decreasing variance as the channel size decreases.

B. Model Assumptions, Limitations and Criticism

Having presented the evidence supporting our modeling approach, we now provide some critical analysis of our assumptions and method. As mentioned, in order to map the detailed WOSM to the one-dimensional dumbbell model, we assumed that small fluctuations about the equilibrium extension were approximately Gaussian. Accordingly, we need information on the probability density function, $\psi(X)$, of the span of the detailed model. Naturally, $\psi(X)$ cannot be exactly Gaussian due to finite extensibility (i.e. X can not exceed L[44]) and hairpin states may cause the distribution to be distinctly non-Gaussian[20,29]. To avoid any complication due to global hairpins[20], we initialized all of our Monte Carlo runs in extended states. Subsequently, while many backfolded states were realized in weak confinement, no global hairpins were detected for $D \lesssim l_p$. This observation is consistent with the hypothesis that hairpin formation is a rare, slow event in Metropolis Monte Carlo simulations of DNA in tight confinement[29]. However, with this method we are unable to determine if hairpins are in fact absent from the equilibrium ensemble, or if the simulation is incapable of reaching the time scale necessary to observe such configurations. Regardless, it seems likely that experimental measures of the relaxation time also neglect hairpins, since they are easily observed[2,27,37,61,62].

Figure 4(a) shows the resulting probability density functions, $\psi(X)$, obtained from the configurations of the WOSM, where the bulk of the probability density is reasonably well approximated as Gaussian for all channel sizes. Indeed, this approximation is further supported by the normal probability plots shown in Fig. 4(b), which show that no significant deviation from Gaussian behavior occurs until ± 2 standard deviations. Since the chain has a finite extension, there must be deviations from Gaussian behavior in the tails of the nor-

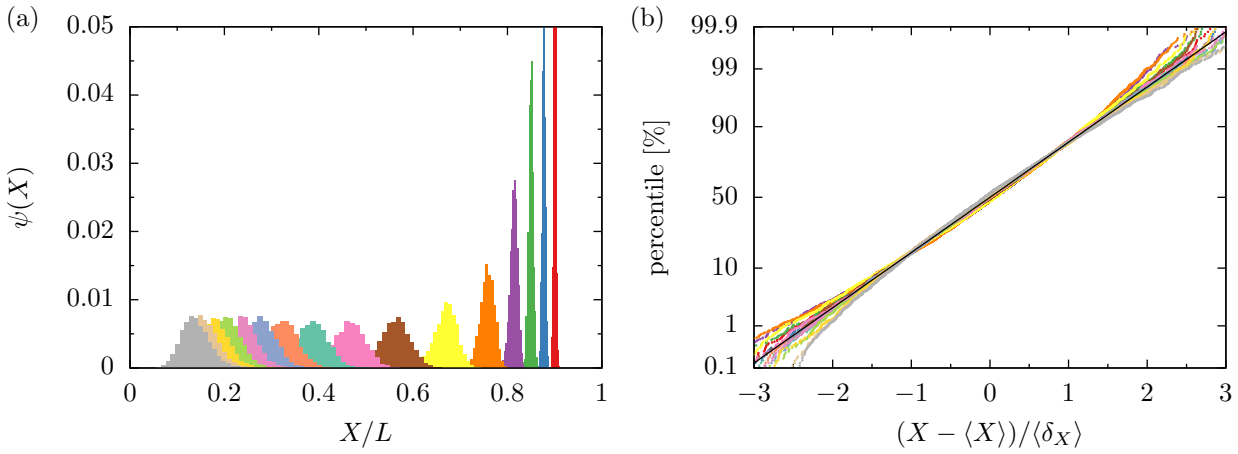

FIG. 4. (a) Probability density function for the chain extension $\psi(X)$ in the WOSM for different channel sizes as a function of fractional extension. The channel sizes shown are (from right to left in nm): 30, 36, 43, 52, 62, 74, 89, 106, 127, 152, 183, 219, 262, 314, 376, 450. (b) Normal probability plot of the 16 distributions. The solid black line indicates a normal distribution. The color scheme in both panels is the same.

mal probability plots. Additionally, note that there is poorer sampling in the tails of the distributions, leading to substantial noise in this region.

Perhaps the most uncertain part of our analysis is the estimation of the various parameters l_p, w, a and even L in the presence of the intercalating dye, which is the main reason why we chose to include a fitting parameter in Eq. 5. Indeed, it seems that all attempts to quantitatively compare simulations and theory to experimental data for DNA are impacted by the absence of reliable measurements for these parameters for dyed DNA.[28] We have adopted the standard approach here, increasing the contour length by 20-30% while assuming the persistence length is unchanged, inspired by the success of these parameters in models for DNA electrophoresis[63].

Given the number of approximations required to reduce an intractable dynamic simulation problem to a feasible Monte Carlo calculation, the quantitative agreement in Fig. 1 is satisfying, especially since all of the uncertainty in the parameters and the assumptions required for the methodology seem to be reducible to a single $O(1)$ fitting constant. In particular, while the Kirkwood approximation is known to be accurate for weak confinement[34], there are no experimental data or dynamic simulation data to assess its accuracy in strong confinement. A possible route to improving the quantitative agreement is to modify the

WOSM so that the spheres correspond to the hydrodynamic diameter a rather than the excluded width w, thereby improving the accuracy of the hydrodynamic calculations while simultaneously reducing discretization artifacts in the smaller channels. However, the trade-off is an increased number of beads required to reach a particular contour length L; the requisite hydrodynamics calculations entail improvements in the methodology that are currently in development. We also recognize the need to develop a more sophisticated model for the DNA-wall interactions in the Odijk regime, where the hardcore excluded volume is probably insufficient.

IV. CONCLUSION

In the present contribution, we showed how a one-dimensional, overdamped, Rouse dumbbell model, parameterized from detailed Monte Carlo simulations, can reasonably reproduce the relaxation time data observed in experiments[37] using a single $O(1)$ fitting parameter. While there are a number of assumptions underlying our analysis, the final result in Fig. 1 suggests that our model is sufficient to capture the extant experimental data. There are two obvious routes to test our approach. One option is to acquire experimental data under the same experimental conditions, since our simulation results make a testable prediction about the shape of the relaxation time curve. However, it seems likely that additional experimental data points would not invalidate our result, especially in light of the experimental uncertainties. A more promising avenue is to acquire experimental data for the relaxation time at different ionic strengths, which will alter simultaneously the persistence length and the effective width[56,64,65]. Inasmuch as we have already used our adjustable parameter in Eq. 5, changing ionic strength would provide a stringent test of our approach. Naturally, we would also need to recompute the data in Fig. 3 for the new values of l_p and w, but this is a straightforward computational task.

If additional experimental data ultimately point out a shortcoming in our result, it is worthwhile to consider what might be the weakest link connecting the detailed Monte Carlo simulations to the relaxation time. Based on Fig. 4, it would seem that the assumption of a Gaussian spring for the fluctuations about the equilibrium extension is a possible source of error. While the bulk of the probability distribution is captured by a Gaussian distribution, the tails certainly cannot be Gaussian. Moreover, depending on the amount of weight in

the tails, they may make a non-trivial (but still finite) contribution to the variance in the extension. Fortunately, there is already a body of literature on polymer rheology using dumbbell models with more sophisticated spring laws[47]. Moreover, one should be able to construct an appropriate spring by comparing its thermal properties to the histograms in Fig. 4. While any such model is certainly more complicated than the Gaussian model we used here, the additional degrees of freedom in a more complicated spring law — along with a finite extensibility — should improve the agreement with experimental data.

Moving beyond the methodology, our results suggest that a dramatic reduction in the fluctuations of the span of the chain as the channel size drops below the Kuhn length of the DNA, not the increased friction, are responsible for a qualitative change in the relaxation time. This phenomenon is not just a scientific curiosity; it is critical to the success of state-of-the-art DNA mapping in nanochannels. In the commercial method[6,7], the DNA molecules are decorated with sequence-specific probes and injected into an array of nanochannels. The resulting massively parallel array of linearized molecules is imaged in a series of consecutive scans. The extension fluctuations thus set the lower bound for the error in a single snapshot of the extension between two barcodes. The most recently reported nanochannel mapping device[7] uses 45 nm $\times$ 45 nm channels, which are well below the 100 nm Kuhn length of DNA. Our data suggest that these channel sizes suppress the variance in distance between barcodes, thereby permitting a robust identification of the structural variations that are critical to understanding genomic diversity[7].

ACKNOWLEDGMENTS

This work was supported by the NIH (R01-HG005216 and R01-HG006851) and the NSFC (21204061) and was carried out in part using computing resources at the University of Minnesota Supercomputing Institute. We thank Jay Schieber (Illinois Institute of Technology) for useful discussions, Walter Reisner (McGill University) for providing us with the experimental data in Fig. 1, Han Cao and the technical staff at BioNano Genomics for insights into their genome mapping technology, and Steve Levy (SUNY-Binghamton) for critical comments on our manuscript.

REFERENCES

[1]F. Persson and J. O. Tegenfeldt, Chem. Soc. Rev. **39**, 985 (2010).

[2]S. L. Levy and H. G. Craighead, Chem. Soc. Rev. **39**, 1133 (2010).

[3]W. Reisner, J. N. Pedersen, and R. H. Austin, Rep. Prog. Phys. **75**, 106601 (2012).

[4]K. D. Dorfman, S. B. King, D. W. Olson, J. D. P. Thomas, and D. R. Tree, Chem. Rev. **113**, 2584 (2013).

[5]K. Jo, D. M. Dhingra, T. Odijk, J. J. de Pablo, M. D. Graham, R. Runnheim, D. Forrest, and D. C. Schwartz, Proc. Natl. Acad. Sci. USA **104**, 2673 (2007).

[6]S. K. Das, M. D. Austin, M. C. Akana, P. Deshpande, H. Cao, and M. Xiao, Nucleic Acids Res. **38**, e177 (2010).

[7]E. T. Lam, A. Hastie, C. Lin, D. Ehrlich, S. K. Das, M. D. Austin, P. Deshpande, H. Cao, N. Nagarajan, M. Xiao, and P.-Y. Kwok, Nat. Biotech. **30**, 771 (2012).

[8]C. Zhang, A. Hernandez-Garcia, K. Jiang, Z. Gong, D. Guttala, S. Y. Ng, P. P. Malar, J. A. van Kan, L. Dai, P. S. Doyle, R. de Vries, and J. R. C. van der Maarel, Nucleic Acids Res. (2013), 10.1093/nar/gkt783.

[9]A. R. Hastie, L. Dong, A. Smith, J. Finklestein, E. T. Lam, N. Huo, H. Cao, P.-Y. Kwok, K. R. Deal, J. Dvorak, M.-C. Luo, Y. Gu, and M. Xiao, PLoS ONE **8**, e55864 (2013).

[10]T. Odijk, Macromolecules **16**, 1340 (1983).

[11]J. Wang and H. Gao, J. Chem. Phys. **123**, 084906 (2005).

[12]F. Wagner, G. Lattanzi, and E. Frey, Phys. Rev. E **75**, 050902 (2007).

[13]Y. Yang, T. W. Burkhardt, and G. Gompper, Phys. Rev. E **76**, 011804 (2007).

[14]T. W. Burkhardt, Y. Yang, and G. Gompper, Phys. Rev. E **82**, 041801 (2010).

[15]Y. Kim, K. S. Kim, K. L. Kounovsky, R. Chang, G. Y. Jung, J. J. de Pablo, K. Jo, and D. C. Schwartz, Lab Chip **11**, 1721 (2011).

[16]R. Chang and K. Jo, J. Chem. Phys. **136**, 095101 (2012).

[17]L. Dai, S. Y. Ng, P. S. Doyle, and J. R. C. van der Maarel, ACS Macro Letters **1**, 1046 (2012).

[18]W. F. Reinhart, D. R. Tree, and K. D. Dorfman, Biomicrofluidics **7**, 024102 (2013).

[19]F. Brochard-Wyart, T. Tanaka, N. Borghi, and P.-G. de Gennes, Langmuir **21**, 4144 (2005).

[20]T. Odijk, J. Chem. Phys. **125**, 204904 (2006).

[21]T. Odijk, Phys. Rev. E **77**, 060901 (2008).

[22]C. Zhang, F. Zhang, J. A. van Kan, and J. R. C. van der Maarel, J. Chem. Phys. **128**, 225109 (2008).

[23]P. Cifra, J. Chem. Phys. **131**, 224903 (2009).

[24]P. Cifra, Z. Benková, and T. Bleha, J. Phys. Chem. B **113**, 1843 (2009).

[25]Z. Benková and P. Cifra, Macromolecules **45**, 2597 (2012).

[26]Y. Wang, D. R. Tree, and K. D. Dorfman, Macromolecules **44**, 6594 (2011).

[27]T. Su, S. K. Das, M. Xiao, and P. K. Purohit, PLoS ONE **6**, e16890 (2011).

[28]E. Werner, F. Persson, F. Westerlund, J. O. Tegenfeldt, and B. Mehlig, Phys. Rev. E **86**, 041802 (2012).

[29]P. Cifra and T. Bleha, Soft Matter **8**, 9022 (2012).

[30]D. R. Tree, Y. Wang, and K. D. Dorfman, Phys. Rev. Lett. **110**, 208103 (2013).

[31]C. Manneschi, E. Angeli, T. Ala-Nissila, L. Repetto, G. Firpo, and U. Valbusa, Macromolecules **46**, 4198 (2013).

[32]L. Dai and P. S. Doyle, Macromolecules **46**, 6336 (2013).

[33]M. Daoud and P.-G. de Gennes, J. Phys. (Paris) **38**, 85 (1977).

[34]R. M. Jendrejack, D. C. Schwartz, M. D. Graham, and J. J. de Pablo, J. Chem. Phys. **119**, 1165 (2003).

[35]C. Micheletti and E. Orlandini, Soft Matter **8**, 10959 (2012).

[36]E. Werner, F. Westerlund, J. O. Tegenfeldt, and B. Mehlig, Macromolecules **46**, 6644 (2013).

[37]W. Reisner, K. J. Morton, R. Riehn, Y. M. Wang, Z. Yu, M. Rosen, J. C. Sturm, S. Y. Chou, E. Frey, and R. H. Austin, Phys. Rev. Lett. **94**, 196101 (2005).

[38]D. R. Tree, Y. Wang, and K. D. Dorfman, Phys. Rev. Lett. **108**, 228105 (2012).

[39]J. O. Tegenfeldt, C. Prinz, H. Cao, S. Chou, W. W. Reisner, R. Riehn, Y. M. Wang, E. C. Cox, J. C. Sturm, P. Silberzan, and R. H. Austin, Proc. Natl. Acad. Sci. USA **101**, 10979 (2004).

[40]M. D. Graham, Annu. Rev. Fluid Mech. **43**, 273 (2011).

[41]R. M. Jendrejack, J. J. de Pablo, and M. D. Graham, J. Chem. Phys. **116**, 7752 (2002).

[42]Y. L. Chen, M. D. Graham, J. J. de Pablo, G. C. Randall, M. Gupta, and P. S. Doyle, Phys. Rev. E **70**, 060901(R) (2004).

[43]P. J. Hagerman and B. H. Zimm, Biopolymers **20**, 1481 (1981).

[44]Y. Wang, W. F. Reinhart, D. R. Tree, and K. D. Dorfman, Biomicrofluidics **6**, 014101 (2012).

[45]E. F. Koslover and A. J. Spakowitz, Macromolecules **46**, 2003 (2013).

[46]T. Cui, J. Ding, and J. Z. Y. Chen, Phys. Rev. E **78**, 061802 (2008).

[47]R. B. Bird, C. F. Curtiss, R. C. Armstrong, and O. Hassager, *Dynamics of Polymeric Liquids, Volume 2, Kinetic Theory* (John Wiley & Sons, 1986).

[48]A. Karpusenko, J. H. Carpenter, C. Zhou, S. F. Lim, J. Pan, and R. Riehn, J. Appl. Phys. **111**, 024701 (2012).

[49]T. C. B. McLeish, Adv. Phys. **51**, 1379 (2002).

[50]B. H. Zimm, Macromolecules **13**, 592 (1980).

[51]R. Rodríguez Schmidt, J. G. Hernández Cifre, and J. García de la Torre, Eur. Phys. J. E **35**, 130 (2012).

[52]A. G. Balducci, C. C. Hsieh, and P. S. Doyle, Phys. Rev. Lett. **99**, 238102 (2007).

[53]Y. Wang, I. Teraoka, F. Y. Hansen, G. H. Peters, and O. Hassager, Macromolecules **44**, 403 (2011).

[54]M. Doi and S. F. Edwards, *The Theory of Polymer Dynamics* (Oxford University Press, 1986).

[55]M. Rubinstein and R. H. Colby, *Polymer Physics* (Oxford University Press, NY, 2003).

[56]D. R. Tree, A. Muralidhar, P. S. Doyle, and K. D. Dorfman, Macromolecules (in press).

[57]C. Bustamante, J. F. Marko, E. D. Siggia, and S. Smith, Science **265**, 1599 (1994).

[58]D. Stigter, Biopolymers **16**, 1435 (1977).

[59]J. García de la Torre, A. Jiménez, and J. J. Freire, Macromolecules **15**, 148 (1982).

[60]E. F. Casassa, J. Polym. Sci., Part B: Polym. Lett. **5**, 773 (1967).

[61]S. L. Levy, J. T. Mannion, J. Cheng, C. H. Reccius, and H. G. Craighead, Nano Lett. **8**, 3839 (2008).

[62]J. T. Mannion, C. H. Reccius, J. D. Cross, and H. G. Craighead, Biophys. J. **90**, 4538 (2006).

[63]K. D. Dorfman, Rev. Mod. Phys. **82**, 2903 (2010).

[64]W. Reisner, J. P. Beech, N. B. Larsen, H. Flyvbjerg, A. Kristensen, and J. O. Tegenfeldt, Phys. Rev. Lett. **99**, 058302 (2007).

[65]C.-C. Hsieh, A. Balducci, and P. S. Doyle, Nano Lett. **8**, 1683 (2008).